Synchrotron X-Ray diffraction on individual core/shell $GaAs/In_xGa_{1-x}As$ nanowires at beamline P08 - PETRA III (DESY)

Sean Finn, Trinity College Dublin, Ireland

Supervisor: Dr. Genziana Bussone

September 7, 2017

Abstract

The characterization as well as the structural analysis of core/shell GaAs/InGaAs nanowires is outlined in this report. Advanced characterization methods such as nanobeam focused X-Ray diffraction, in addition to conventional methods such as SEM, EDX, TEM and ensemble XRD (X-Ray Diffraction), revealed useful information about the NW crystal structure. The contemplation of relaxation mechanism and strain analysis of such heterostructures is essential for the development of future nano-based-electronics.

The observation of a particular nanowire and its reciprocal space maps, revealed a strain of $\epsilon_{hkl} \sim 0.004$, which is an encouragingly low value, indicating a promising structural stability of the nanowire in question. This low value is similar to previous ensemble measurements on the same nanowires and indicates the presence of an out-of-plane relaxation of the InGaAs shell crystal lattice. The space maps did not reveal any information about the GaAs core.

Overall this project has been an encouraging experience in the field of material analysis and nanowire characterization. The summer internship has been quite a wholesome experience.

Contents

1 Introduction

1.1 DESY and PETRA III

The construction of the **DESY** (Deutsche Elektronen Synchrotron) began in 1960. Only 4 years later the first electrons were accelerated through the synchrotron, and research on quantum electrodynamics began. Throughout the years, further accelerators were developed, and today, the third installment of PETRA, namely **PETRA III** is one of DESY's most important facilities. Originally built as a storage ring to research elementary particles, fruition of this research came into being upon the discovery of the mediating gluon particle in 1979. Later, PETRA was adopted as a pre-accelerator for the **HERA** storage ring, and thus became **PETRA II**. After the shutdown of HERA in 2007, PETRA III has capitalized upon synchrotron radiation, and is now one of the most brilliant sources of synchrotron radiation. Annually, hundreds of users from all around the world use the PETRA III facility, and as such, DESY has established good connections with other institutions throughout the world.

In 1968, the DESY Summer Student Program was enacted. Now, some years later, I have the fortunate opportunity to be enrolled as a Summer Student myself. I have had the great opportunity to work at one of the most impressive research facilities all over the world. As member of the team of the High Resolution X-ray Diffraction beamline P08, I have engaged with various scientists, regularly attended constructive meetings, and enjoyed the social aspect of a synchrotron environment at PETRA III.

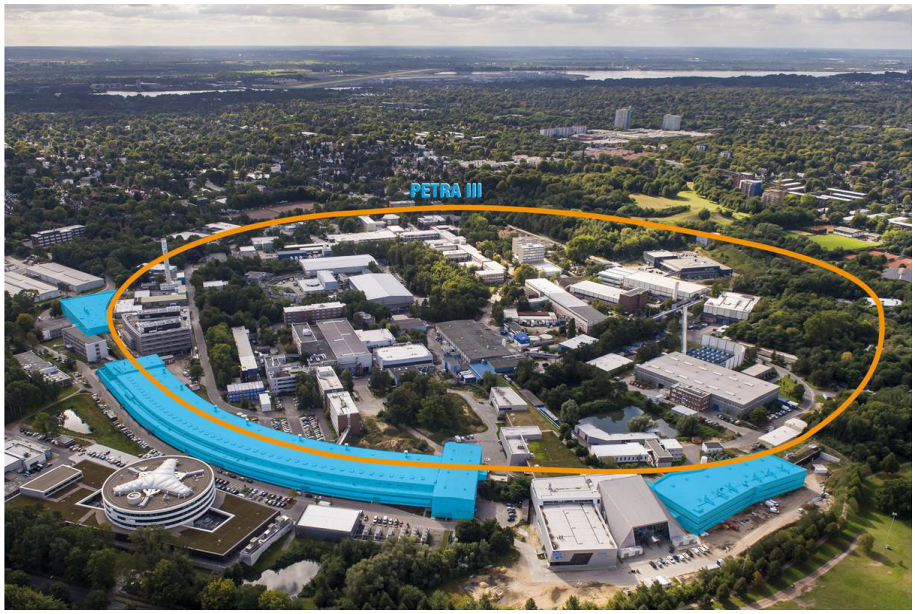

Figure 1: An image of PETRA III [**1**]

1.2 Aim of the Project

As a participant of the DESY Summer Student program, I had the pleasure of working with Genziana Bussone. Genziana works on High Resolution X-Ray Diffraction at the P08 Beamline of PETRA III, and I have worked on the first nano-XRD (X-ray Diffraction) data set collected at beamline P08 on individual **Nanowires (NW)** (PETRAIII Experimental report I-20160337). This characterization has been achieved by making use of a recently developed nano-focused X-ray beam experimental configuration. The goal of my project was to investigate the axial strain distribution and polypypism in individual free-standing core/shell NWs on their original growth Si substrate. In the material system under investigation, preliminary **XRD (X-ray Diffraction)** measurements on ensemble NWs suggest the presence of a strong tensile strain in the core for a particular shell thickness, as a result of the small dimensions of the core (25 nm in diameter). Here, the dependence of the strain level on the shell composition and thickness opens new ways towards strain engineering in core/shell NWs.

However, the average character of the XRD ensemble measurement does not provide information about inhomogeneities along the growth axis of individual NWs, neither about structural differences between nano-objects within the same substrate. In this context, the characterization of individual NWs plays a crucial role.

In addition to my scientific project, I was given the opportunity to work at Beamline P08, actively conducting X-Ray Diffraction ensemble characterization on further samples.

1.3 What are Nanowires?

The assurgence of research into NWs in recent years, has exposed them to be a very promising alternative to thin film technologies. NWs have been shown to have exceptional physical responses, such as mechanical, electrical, optical properties. What makes NWs unique is that such properties are not observed within a bulk of these materials. These arguments outline NWs as highly suitable for the integration into electronic and photonic nanoscale devices, such as transistors, lasing devices, LEDs etc .A wide range of suitable materials exist for the growth of NWs, however the NWs under characterization, consist of a GaAs core with an InGaAs exterior shell. The general formula for these NWs is $GaAs/In_xGa_{1-x}As$, where 'x' is a composition variable. These NWs are grown by Molecular Beam Epitaxial on a Silicon substrate.

GaAs, like many other NW materials, is a semiconductor. In nanostructures it, can adopt two possible polytype structures, Wurzite **(WZ)**, which is derived from the HCP unit cell, and Zincblende **(ZB)** which comes from the FCC structure. Both of these polytypes have demonstrated different physical properties, the ZB GaAs polytype has shown a nominal band gap of $E_g = 1.42eV$ **[2]** in bulk material, whereas the WZ structure has a energy gap of $E_g = 1.46eV$. **[3]**. In NWs, the high aspect ratio compared to

the bulk material has a large impact upon the electrical parameters of these materials, such as mobility of charge carriers and resistivity, which may change by several orders of magnitude.

Figure 2 demonstrates the basic dimensions of the NWs under inspection. Figure 3 is a simulated visualization of an ensemble of NWs embedded on a Si substrate, not to scale.

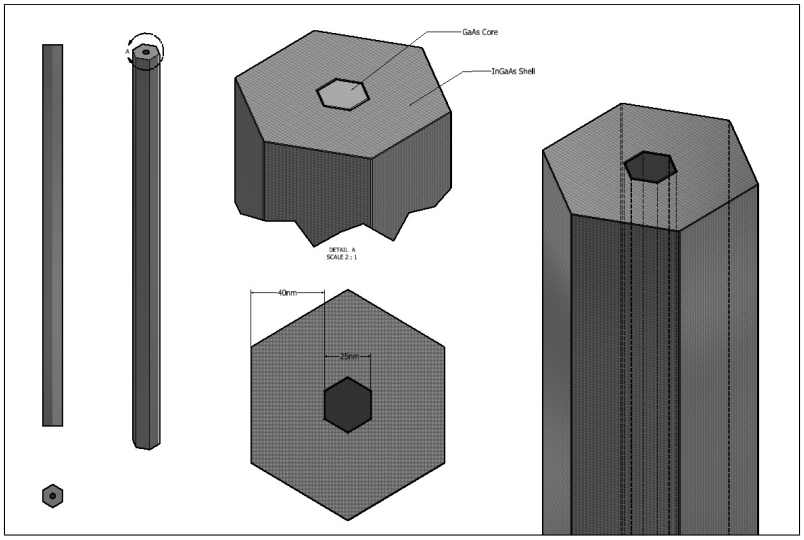

Figure 2: Basic dimensions of $GaAs/In_xGa_{1-x}As$ NWs

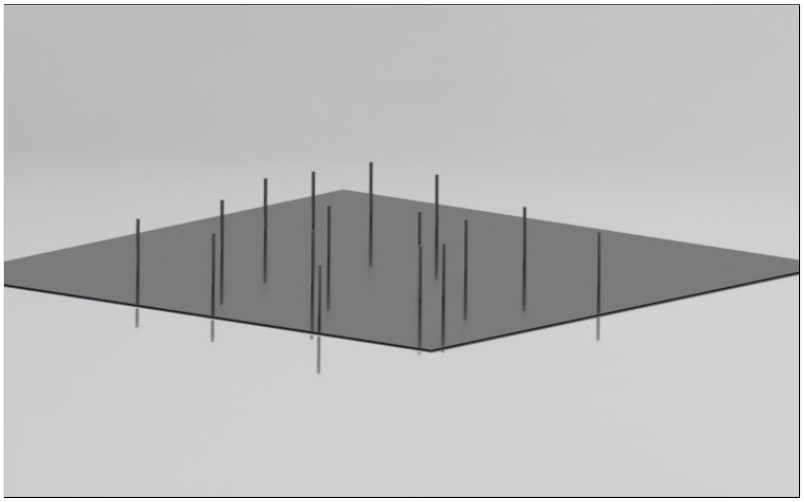

Figure 3: Recreated image of an ensemble of NWs on Si substrate

2 Theory

2.1 Reciprocal Space, X-Ray Diffraction

XRD has become a very popular and effective characterization technique in solid state physics. It allows for the 3D visualization of electron density, which in turn allows for the determination of the atomic and molecular structure of crystalline structures.

A good starting point for the understanding of XRD, is the simple definition of a crystal, that is; the three dimensional periodic repetition of a basic structural repeating unit. This so called "Repeating unit", is essentially, the fundamental building blocks of any crystal, and is known as the **Primitive Unit Cell (PUC)** , it is defined by it's **Basis Vectors**: $\vec{a_1}, \vec{a_2}, \vec{a_3}$. The mathematical description of a crystal, that is a set of discrete points which define the geometry of its atomic structure, is known as the **Crystal Lattice**. Translation of the PUC, along it's basis vectors to all lattice points, results in the generation of a crystal. The distance of a given PUC from the origin of the crystal, is defined by the vector $\vec{r_n}$. The geometric position of the n^{th} atom relative to the origin of the crystal is thus defined by:

$$\overrightarrow{R_m^n} = m_1\vec{a_1} + m_2\vec{a_2} + m_3\vec{a_3} + \vec{r_n} \tag{1}$$

m_1, m_2, m_3 are integer numbers specific to a certain atom, however as can be seen in Equation 1, the basis vectors are the same for each atom, which demonstrates the periodicity of the crystal structure. The set of lattice vectors $\vec{R}$ which define the crystal lattice are defined by:

$$\overrightarrow{R_m} = m_1\vec{a_1} + m_2\vec{a_2} + m_3\vec{a_3} \tag{2}$$

This periodic nature of a structure, allows for the identification of lattice planes. These are parallel planes, the orientation which is defined by the **Miller indices (hkl)**. Families of parallel lattice planes are defined by hkl. In HCP structures, the lattice planes are denoted by (hkil), where $i = -h + k$.

Having an understanding of the lattice planes of a crystal, allows the calculation of the inter-planar distance d_{hkl}, which is an important variable in order to comprehend the crystal structure. It is defined in Equation 2,where 'a' is the lattice parameter of the crystal, as:

$$d_{hkl}^{cubic} = \frac{a}{\sqrt{h^2 + k^2 + l^2}} \tag{3}$$

Another important concept, crucial in understanding XRD, is the idea of **Reciprocal Space**. We have already defined a crystal lattice with a set of vectors $\vec{R}$ in **Real Space**, there exists a set of reciprocal lattice vectors $\vec{G}$ in Reciprocal Space, such that the condition $e^{i\vec{G}.\vec{R}} = 1$ is satisfied. As in real space, we also have basis vectors $\vec{b_1}, \vec{b_2}, \vec{b_3}$ in reciprocal space, and we can define the reciprocal space vector as:

$$\vec{G} = h\vec{b_1} + k\vec{b_2} + l\vec{b_3} \tag{4}$$

This vector is perpendicular to the hkl lattice planes, and has a magnitude defined by:

$$\vec{G} = \frac{2\pi}{d_{hkl}} \tag{5}$$

Crucial in the understanding reciprocal space, is the literal inversion of space. This is clearly shown in Equation 5, for a large value of d_{hkl}, $\vec{G}$ will be small and vice-versa.

XRD involves the scattering of X-Rays as they interact with the crystal structure of a solid. For nanostructures such as the ones considered in this report, many effects are negligible, such as absorption, Auger emission, and it is approximated that incident Intensity is uniform throughout. The elastic scattering of electrons, where the phase of the scattered waves sums up coherently, produces intense signals, known as **Bragg peaks**. The positions of those signals, are determined by the condition $q = \vec{G}$. [**5**]

In equivalent terms, in the Bragg la w, the requirements for constructive interference are satisfied if the following condition is met:

$$n\lambda = 2d_{hkl}sin\theta_B \tag{6}$$

where n is an integer number, indicating the diffraction order, λ is the wavelength of the incoming X-Rays, and θ_B is the Bragg angle. Equation 6 is known as the **Bragg Equation**.

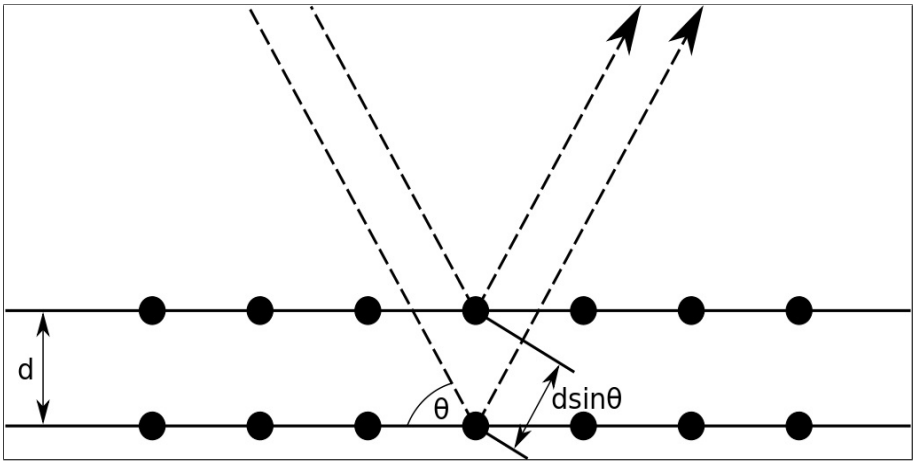

Figure 4: Visualization of Bragg reflection [**7**]

Bragg diffraction is easily interpreted if every atom is considered to be a secondary X-Ray source. That is, each atom will diffract the incident X-Ray. As demonstrated in Fig. 4, some of the incoming X-Rays will be specularly reflected upon impact on the crystal surface, whereas others penetrate further to the next lattice plane and are

diffracted there etc. If the crystal lattice planes are separated by an inter-planar distance d_{hkl}, then it is obvious that the path difference between two coherent X-Rays will be $2dsin\theta$, where θ is the Bragg angle.

In practice, a diffraction pattern is collected by varying θ_B, this is done by rotating the sample platform on the diffractometer, and observing the diffracted X-Rays with the detector.

2.2 Strain and Stress

Defects and aberrations of perfect order within a crystal, will result in unbalanced forces and strain on the NWs. It is therefore desirable to analyze strain distribution, in an attempt to control its structure since the growth and tune the resulting physical properties. The strain ϵ can be expressed in a general form of Hookes' Law:

$$\epsilon_{ij} = S_{ijkl}\sigma_{kl} \tag{7}$$

Where ϵ_{ij} are the strain components, S_{ijkl} are crystal specific coefficients, and σ_{kl} are the components of stress. This equation can equally be expressed as:

$$\sigma_{ij} = C_{ijkl}\epsilon_{kl} \tag{8}$$

where C_{ijkl} is an elasticity matrix.

In order to determine the strain in a NW, it is necessary to consider the ideal structure of the corresponding unstrained crystal lattice. Any strain on the NW will ultimately impact the diffraction pattern, by broadening or shifting peaks, lowering or increasing intensity etc. And as such there will be a difference between theoretical/unstrained and observed/strained crystal lattice.The effective strain on a NW is given by:

$$\epsilon_{hkl} = \frac{d_{hkl,strained} - d_{hkl,unstrained}}{d_{hkl,unstrained}} \tag{9}$$

In Equation 9, $d_{hkl,strained}$ will be calculated using Equation 5. $\vec{G}$ will be determined by the peak position in reciprocal space, this will vary for different signals, and will be an important part of the analysis, determining which component of the NW or perhaps the Si substrate is responsible for which signal.

3 Experimental Details

3.1 Sample Preparation

The NW samples were grown on a Si substrate by **Molecular Beam Epitaxy (MBE)**. MBE is a very popular method for growing Group III-IV semiconductor NWs, and there are two types of growth: catalyst-assisted and self-assisted growth. For the former method, the NWs are grown in the presence of a catalyst material, such as Au. The Au is pre-deposited as a thin film on the Si substrate, which forms Au droplets, which are ideal sites for nucleation of NW growth. The growth elements, Ga and As are diluted in a liquid Au droplet in the vapor phase, and grow as solid GaAs at its bottom. This method is referred to as the **Vapor-Liquid-Solid (VLS)** mechanism. [**8**]

For the case of self-assisted growth, growth takes place in the presence of a liquid droplet of the group III element, in this case Ga, onto a SiO_2 layer, of thickness of tens of nm, which was previously deposited on the growth wafer. Defects within the surface of the SiO_2 layer, act as potential nucleation sites for the liquid droplets, which interact with the vapor content, resulting in NW growth.[**9**]

The GaAs/InGaAs core/shell NWs have been grown using the self-assisted growth method at the Institute of Ion Beam Physics and Materials Research, Helmholtz-Zentrum Dresden-Rossendorf, in Dresden. The nanostructures are (111) oriented and are free-standing on a Si substrate.

Three samples, A,B, and C, with different shell thickness and In content, and same core diameter (25 nm) have been characterized. Sample A and B have a shell thickness of 40 and 80 nm respectively and an In concentration of 16%; sample C has a shell thickness of 40 nm and an In concentration of 45%.

The radial heterostructures are randomly grown on the substrate with a number density of about $10^8 cm^{-2}$. In view of the nano-XRD characterization, this highly 'populated' sample configuration requires a specific sample preparation using an SEM/FIB dual system.

3.2 Sample preparation SEM/FIB

After the growth of the NWs a special sample preparation was conducted using SEM/FIB analysis. **Scanning Electron Microscopy (SEM)** is an electron microscope which produces images of a sample, and allows for detailed investigation of its topography. **Focused Ion Beam (FIB)** ablation, is the removal of material from the surface of a sample using a focused beam of ions. The intention of using these two analytical techniques, was to find individual NWs which were isolated enough from the other NWs, such that they could be characterized independently of any other NWs. Once a suitable candidate was found, it was identified using an 'L' shaped marker, which was physically

engraved about 40 um away from the chosen NW using a FIB. This allowed for easy identification when conducting the XRD experiment.

Figures 5 and 6 show images of the SEM/FIB analysis. Figure 5 shows a large group of NWs on sample A. The NW highlighted in the center is a NW from sample A, and will scrutinized later on regarding its structural integrity. Figure 6 is from a different sample, and demonstrates how a FIB marker may be used to locate an individual NW more easily during XRD analysis.

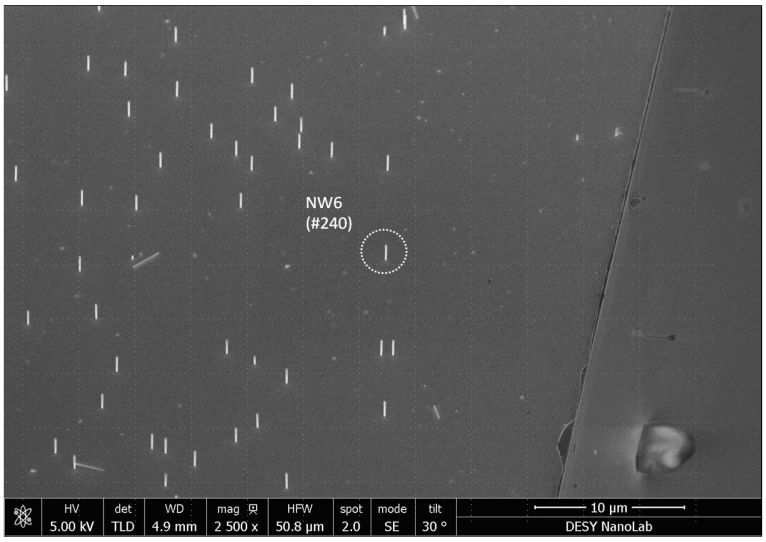

Figure 5: SEM image of an ensemble of NWs on a Si substrate

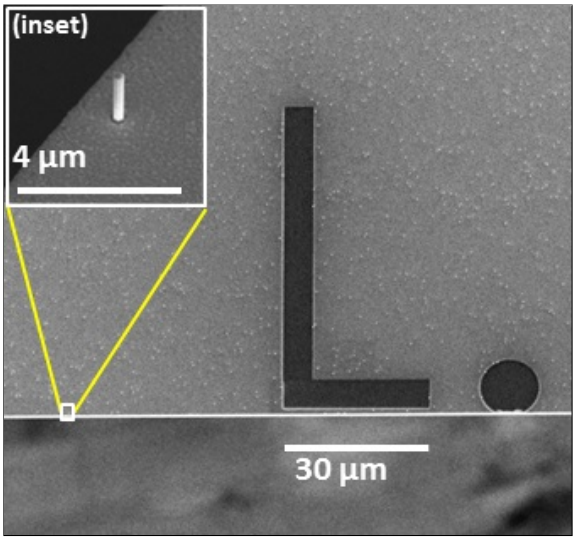

Figure 6: Image of a NW marker

3.3 P08 Beamline, Beam parameters

Nano-focused beam XRD was performed at the High Resolution X-ray Diffraction P08 beamline, located in the PETRA III hall. At an energy of 9keV, the X-ray beam was focused down to a size of $0.4\mu m(V) \times 1.50\mu m(H)$ with a set of Be compound refractive lenses ($N = 45, radius = 0.1\mu m$). With this beam size it is possible to illuminate and characterize an individual NW.

The sample was mounted on a three axes piezo-positioner with a travel range of $38\mu m$, fixed on the goniometer stage of the KOHZU Diffractometer, and the XRD diffraction pattern was measured using the Pilatus 300K detector which was mounted on the detector arm. An in-situ optical microscope mounted on top of the sample on the diffractometer was used to visualize the sample surface and locate the individual nanowires identified by the L shaped markers prepared by FIB. Subsequently, line scans in real space have been performed under Bragg condition, to determine the position of the interesting nanostructures. The (111) symmetric out-of-plane reflection was collected for 2 to 3 NWs in all samples.

4 Data Extraction and Analysis: Reciprocal space maps

4.1 Reciprocal Space Maps

The out-of-plane symmetric reflection (111) was collected for several NWs in sample A, B and C. Transversal scans in reciprocal space have been recorded by varying the sample angle (Bragg angle) for specular diffraction as described in the theory section.

The raw output data from the XRD scan was accumulated as ".tif" detector images. In addition the ".fio" files provide the parameters of each scan; such as the **ROI (Region of Interest)**, the parameters of different motors on the KOHZU diffractometer etc. The data was extracted and converted into reciprocal space using the 'Xrayutilities' package for Python [**4**]. Figure 7 shows a ".tif" image; it can be considered as a slice of a reciprocal space map, associated with a specific Bragg angle.

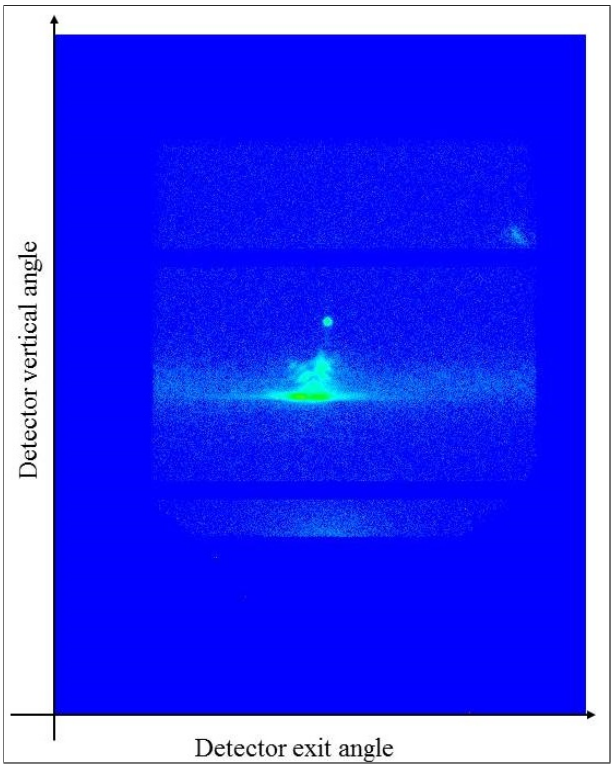

Figure 7: A typical example of a ".tif" file

A particular NW was selected for analysis. Figure 8 shows two-dimensional cuts of the calculated 3D reciprocal space map: from left to right $Q_x, Q_z Q_y, Q_z and Q_x, Q_y$. The vertical bright line in the two dimensional Q_x, Q_z reciprocal space map, originates from the substrate surface and is known as CTR (Crystal Truncation Rod) [**5**]. In both the

Q_x, Q_z and the Q_y, Q_z, there is a high intensity signal at about $1.90(1/\mathring{A})$. By comparison, looking at Q_x, Q_y, providing a top view of the reciprocal space map, one can distinguish at least two signals. The source of two signals rather than one, is a point of interest for this research, as it is not necessarily expected; this will be discussed in further detail later.

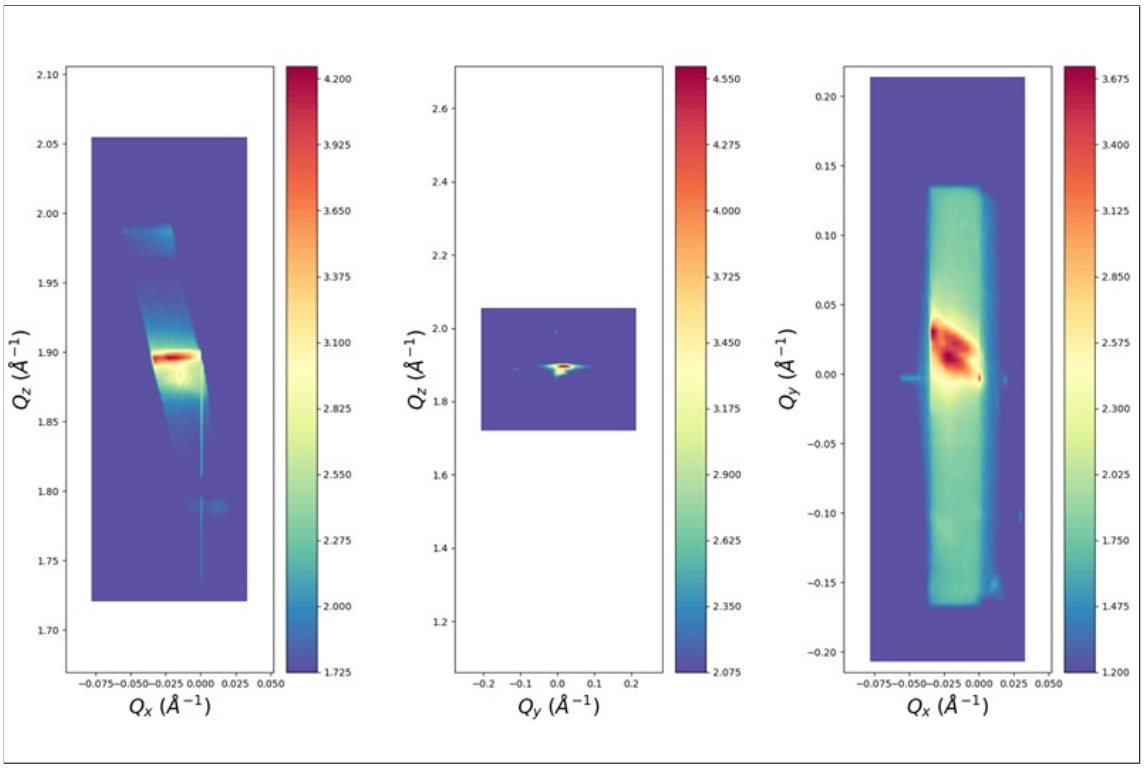

Figure 8: Full reciprocal space map of Sample A

Figure 9 and Figure 10 show different slices of the full reciprocal space maps of sample A. Figure 9 focuses on the upper section of the Q_z axis, where as Figure 10 looks at the lower section. Dividing these parts allows for easier analysis of less intense signals, as the more intense signals are removed and thus weaker, contributing signals are more prominent. For example, approaching this idea by looking at the Q_x, Q_z of both the upper and lower maps, one can identify that the broad signal established in the Q_x, Q_z full map, can actually be separated into two contributing signals, an upper at about $1.90(1/\mathring{A})$ and a lower at about $1.88(1/\mathring{A})$ respectively. In particular the lower signal is underrepresented in the full map of Q_x, Q_z. Moreover, in Figure 8 the Q_x, Q_y map shows the presence of one signal only, which can be attributed to the $GaAs/InGaAs$ material (together with the sharp signal at Q_x $0, Q_y$ 0 originating from the Si CTR).The intensity profiles will provide more clarity.

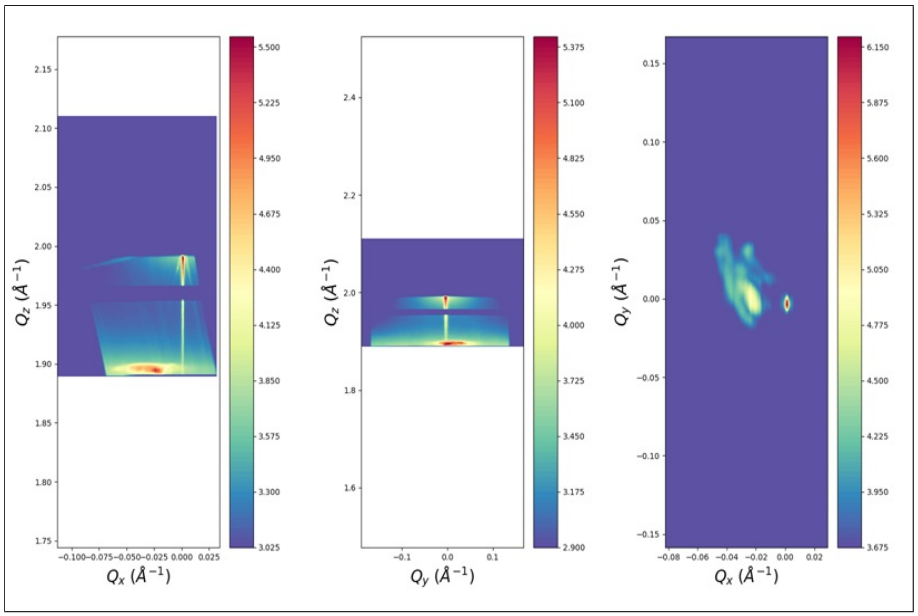

Figure 9: Upper section of the reciprocal space map of Sample A

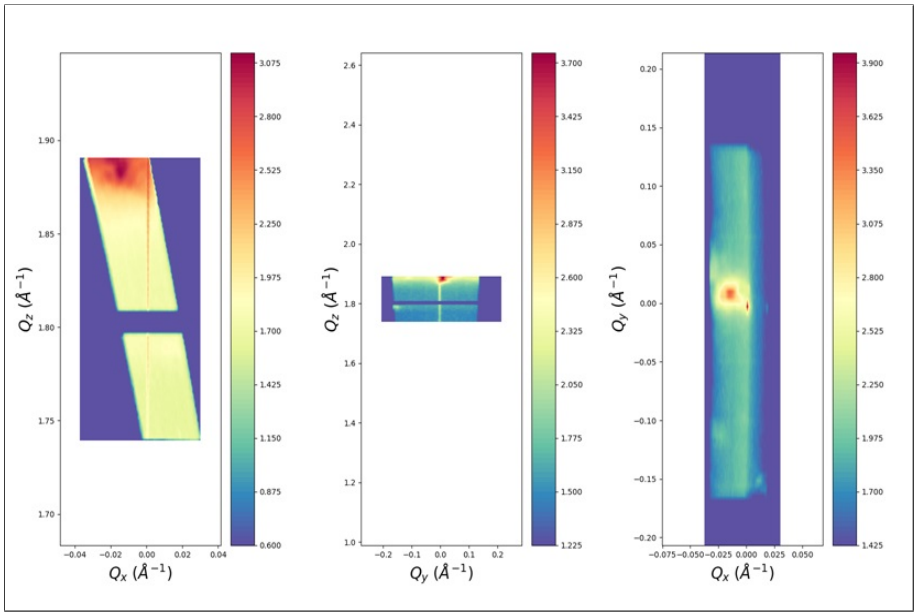

Figure 10: Lower section of the reciprocal space map of Sample A

Next intensity profiles of detected Intensity vs. Q_z position in reciprocal space were calculated to analyze the individual signal peaks. A specific region of reciprocal space was selected around the diffraction signal, in order to isolate it and examine it individually, and the integrated intensity was plotted as a function of the Q_z axis.

Figure 11 shows the intensity profile for the Si substrate. The primary thing to note is the sharpness of the peak, indicating that there are little or no defects in the Si structure.The peak conforms to a Gauss distribution, of which the center is located at 2.004 ± 0.002, see Table 1.

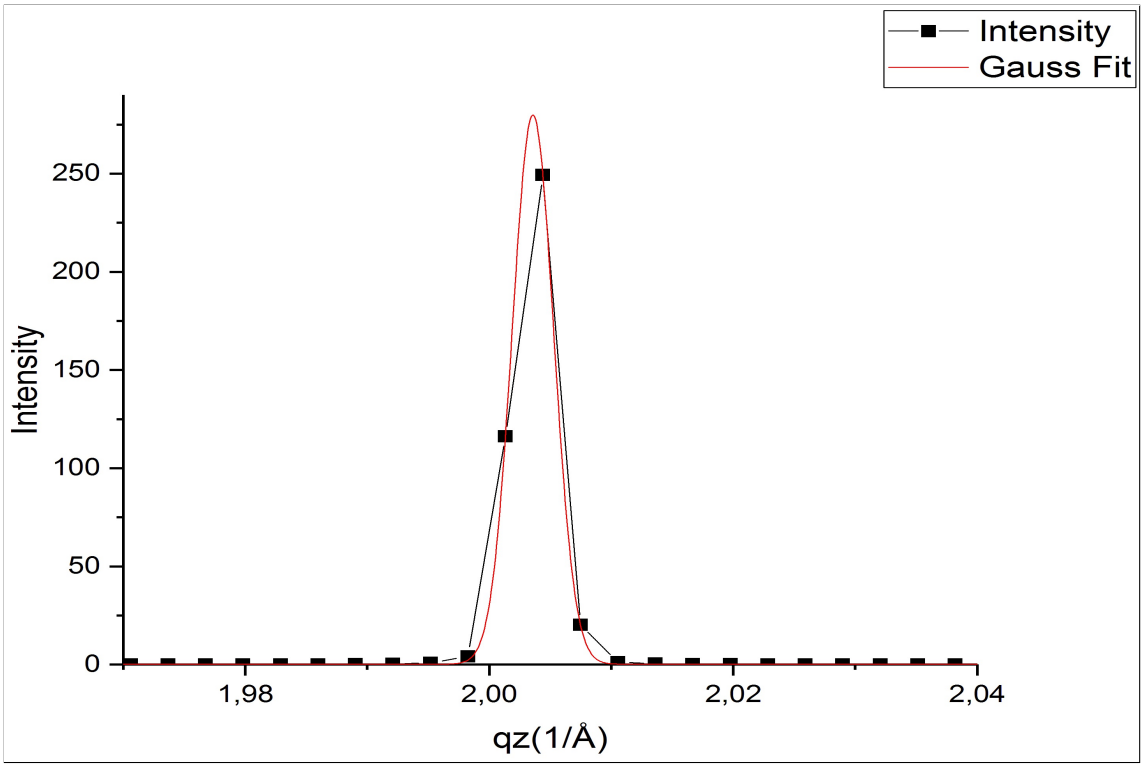

Figure 11: Intensity vs. Q_z position

Next the profile for the GaAs/InGaAs NWs was fitted using two fitting methods, Gauss fitting as seen in Figure 12, and Pseudo Voigt 2 (PsdVoigt2) fitting as seen in Figure 13. A PsdVoigt2, is a curve combining a Gaussian and a Lorentzian distribution: the two functions are summed and their contribution is determined by a 'weighting' parameter μ. In the presented case, both diffraction signal are well represented by one PseudoVoigt curve respectively, with a fixed value of μ.

From the comparison of the Gaussian and Pseudo Voigt fit results, the Pseudo Voigt fitting procedure has been selected as more reliable. The center of the intensity peaks is better represented in the second case, together with the modeling of the FWHM (Full Width at Half Maximum), which includes the tails of both peak contributions.

As mentioned, the presence of two peaks in the Q_z direction is something worth analyzing. Both fits of upper and lower signals are reasonable, and provide meaningful information about spread of the peak, the peak center, which will be useful in

determining whether there are any unresolved stresses on the NW.

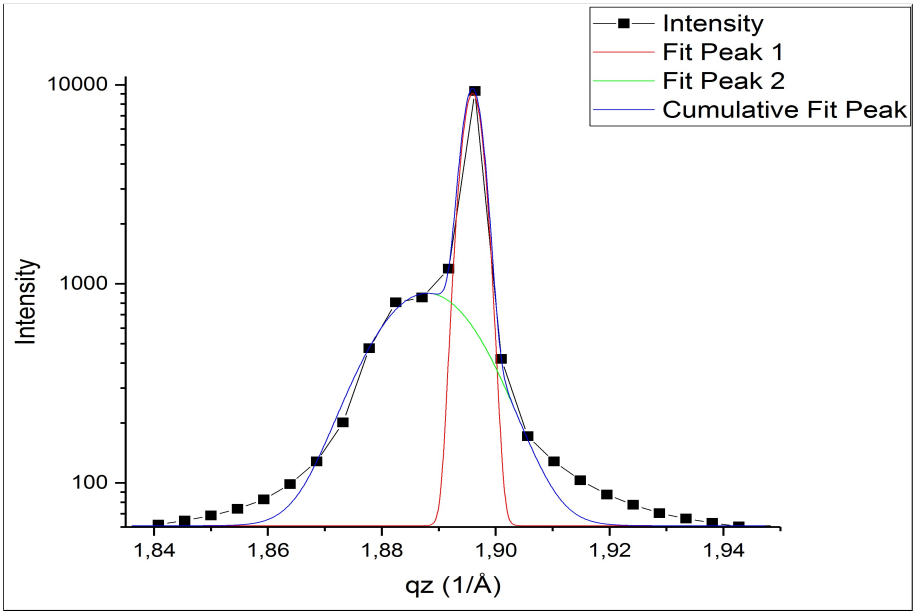

Figure 12: Intensity vs. Q_z position and Gauss fit

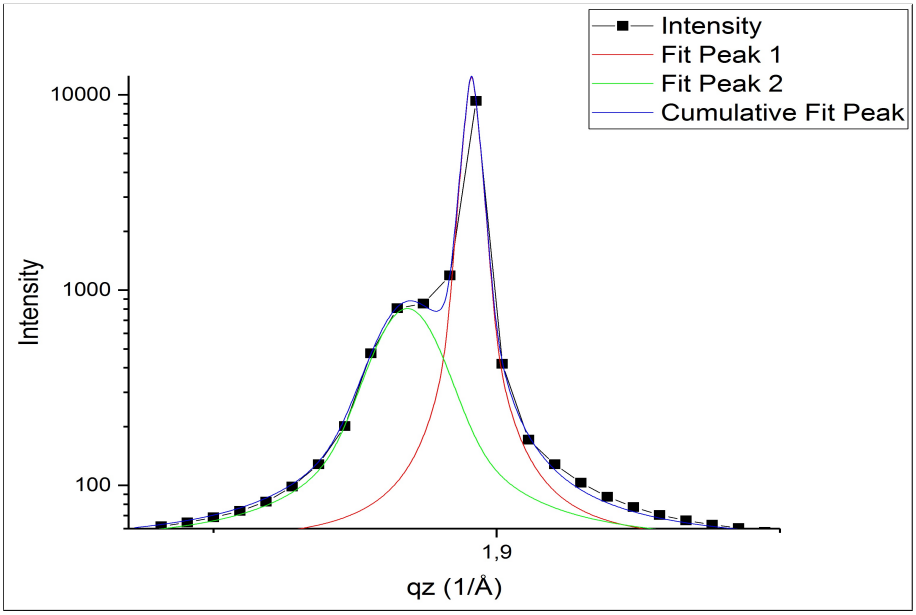

Figure 13: Intensity vs. Q_z position and PsdVoigt2 Fit

Table. 1 provides information about various signals from the Si substrate, as can be seen, the position of the peak, the FWHM, and the standard deviation σ, maintain

almost identical values for each measurement. This is in line with the careful sample alignment performed during the measurements and will constitute our reference in reciprocal space. Tables 2, 3, and 4 provide information about the data analysis for the Samples A, B, and C NW measurements respectively. Analysis of peak positions and comparing them to the theoretical/unstrained values, will allow for insightful strain analysis.

Silicon Intensity Profile			
Sample# Scan#	Position of Peak (1/Å)	FWHM (1/Å)	$\sigma(1/\mathring{A})$
Sample A Scan232	2.004	0.004	0.002
Sample B Scan26	2.004	0.004	0.002
Sample C Scan272	2.004	0.005	0.002

Table 1: Intensity profile Data for Si substrate

Sample A NW Intensity Profiles				
Scan#	Number of Peaks	Fit	Position of Peak 1 (1/Å)	Position of Peak 2 (1/Å)
240	2	Gauss	1.896 ± 0.002	1.888 ± 0.002
240	2	PsdVoigt2 $\mu = 0.6$	1.896 ± 0.002	1.884 ± 0.002
251	2	PsdVoigt2 $\mu = 0.7$	1.895 ± 0.002	1.880 ± 0.002
256	2	PsdVoigt2 $\mu = 0.75$	1.894 ± 0.002	1.882 ± 0.002

Table 2: Intensity profile Data for sample A NWs

Sample B NW Intensity Profiles				
Scan#	Number of Peaks	Fit	Position of Peak 1 (1/Å)	Position of Peak 2 (1/Å)
80	2	PsdVoigt2 $\mu = 0.55$	1.895 ± 0.002	1.884 ± 0.002
138	2	PsdVoigt2 $\mu = 0.35$	1.895 ± 0.002	1.880 ± 0.002

Table 3: Intensity profile Data for sample B NWs

Sample C NW Intensity Profiles				
Scan#	Number of Peaks	Fit	Position of Peak 1 (1/Å)	Position of Peak 2 (1/Å)
300	2	PsdVoigt2 $\mu = 0.85$	1.861 ± 0.002	1.843 ± 0.002
309	2	PsdVoigt2 $\mu = 0.85$	1.860 ± 0.002	1.843 ± 0.002
323	2	PsdVoigt2 $\mu = 0.8$	1.860 ± 0.002	1.843 ± 0.002
327	2	PsdVoigt2 $\mu = 0.6$	1.858 ± 0.002	1.837 ± 0.002

Table 4: Intensity profile Data for sample C NWs

4.2 Individual Nanowires Strain Analysis

The strain on an individual NW will be determined by comparing the theoretical and unstrained center of peak positions to the experimental strained positions. As mentioned before, the NW signal contains two distinguishable peaks. It is important to note that the higher intensity peak, was clearly observable for the signal which was elicited from an ensemble of NWs. So it can be said with certainty that this signal is produced by the NW, and thus will be used to calculate strain. The origin of the lower intensity peak will be discussed later.

Sample A scan 240 will be focused on for strain analysis, but in principle the same calculations could be carried out for each NW. For sample A, previous EDX measurement on the same sample revealed 16% average In concentration in the shell of the heterostructures, such that the structure can be defined as $In_{0.16}Ga_{0.84}As$. Assuming as known the In composition of the NWs, the center of the peak positions from scan240, and Eq. 9 from the Theory section, one can easily determine the strain on a NW.

Firstly, a presumption is made, the material constituting the Si substrate is unstrained and any deviation from its theoretical position in reciprocal space is due to a sample misalignment: the associated shift present in the Si reciprocal space map peak,will therefore also affect the NW position. The Si substrate corresponding to scan240, is sample A scan232. This shift, α,is defined as:

$$q_{Si,theoretical} - q_{Si,real} = \alpha \tag{10}$$

$q_{Si,real} = 2.004$, is the experimental value of the peak position as demonstrated in Table. 1. $d_{Si,hkl,theoretical}$ was calculated using Eq. 3, with the lattice parameter **a**, sourced from an online database. [**6**]. After this $q_{Si,theoretical}$, that is, theoretical reciprocal space vector, was determined using Eq. 5, as $q_{Si,theoretical} = 2.004 \pm 0.0017(1/\mathring{A})$. Hence α was found to be $\alpha = -1.71 \times 10^{-4}$. However, the calculated value is one order of magnitude lower than the estimated uncertainty of the peak position. In this case, the correction can therefore be omitted, as the real and theoretical values of the Si peak position are equal.

Similarily as before, the theoretical position of the NW peak was calculated using the online database considering the composition of the NW, and Eq. 3, $q_{NW,theoretical} = 1.903(1/\mathring{A})$. Following the calculation presented before for the Si substrate, no correction needs to be applied to the position of the NW signal. Using Eq. 3, $d_{NW,hkl,theoretical} = 3.302(\mathring{A})$ was determined for the theoretical/unstrained position. Finally, using $q = 1.896 \pm 0.002(1/\mathring{A})$ from the experimental, $d_{hkl,strained} \sim 3.314(\mathring{A})$ was determined.

Thus, using 5 the effective Strain is $\epsilon_{hkl} \sim 0.004\%$. This procedure could be repeated

for the remaining scans, however this is simply a exemplary exercise.

4.3 What next? Discussion and Outlook

This XRD experiment focused on the structural analysis of individual NWs.The reciprocal space maps for sample A scan240 demonstrated quite uniform signals.

The strain calculation on sample A scan240 revealed a strain value of$\sim$ 0.004%. This low value is compatible with previous ensemble measurements on the same NWs and indicates the presence of an out-of-plane relaxation of the InGaAs shell crystal lattice. No signal from the very thin GaAs core were detected in any of the NWs at the relaxed GaAs position, this follows then as well as the conclusions obtained from previous ensemble characterizations.

Upon closer inspection, two separate diffraction signals close to the InGaAs position were identified in reciprocal space along the growth axis of the NW. The origin of the signal at lower Q_z values could be attributed to the presence of WZ polytype or a different In concentration in part of the NW structure. On the other hand the signal could arise as well from small crystallites grown (as a side effect of the NW growth) on the sample surface in the area within 5 to 10 um from the NW position. The attribution of this second signal is at the moment unclear and requires further investigations.

For this purpose a nano-XRD beamtime has been allocated at beamline ID01 at the ESRF in Grenoble in October 2017.

5 Complementary Activities

This section contains additional work and experience I gathered during my stay at DESY.

5.1 Ensemble Nanowire Measurements and P08 Beamline

Using a hundreds micron sized beam with a X-ray energy of 9keV, an ensemble of GaAs NWs was characterized at the P08 beamline.The average structure of ensemble NWs with two different shell thickness (20 nm and 40 nm) and the same core diameter (25 nm) has been investigated using XRD. I first performed a conventional alignment procedure, to center the sample vertically into the X-ray beam and to set the incident angle of the X-ray beam to the sample surface to 0. Then I have collected the (111) symmetric and the (422) asymmetric out-of-plane reflections for both samples.

5.2 FIB/SEM Characterisation

A peculiar sample preparation, in view of a beamtime allocated at the ESRF in Grenoble (France) in October 2017, has been carried out in the DESY Nanolab. Several individual NWs were located in a dual SEM/FIB system, and marked using an 'L' shaped identifier, which was milled into the sample using a FIB. The same sample preparation has been performed for the nano-XRD characterization at beamline P08.

5.3 Von Laue under High Pressure

As part of an "Exercise Day", I was given the opportunity with some of my fellow students to take part in an additional small project. Our group had the fortunate luck of conducting Von Laue diffraction on a sample of germanium under various high pressure conditions. The aim of the experiment was to determine the structural changes of Ge under different conditions of pressure and temperature, and to observe the phase changes of Ge. The experiment was conducted at the P02 beamline, and the results were presented to a group 20 students.

5.4 Exchange with International Summer Students

The interaction and exchange with other Summer students from all places of the globe has been perhaps one of the most insightful experiences I have had during my stay at DESY. New friends were made, new cultures, idioms, languages, ideas and passions were discovered and shared. I have seen more of the world in these few weeks than some might see their entire life, and with that, it has been a truly memorable experience.

6 Conclusion

The future of nanoelectronics is in good hands with progress and improvements being made all the time. In this context, great interest is given to the tuning and understanding of semiconducting NW structure and their resulting physical properties. In my report I presented the characterization and data analysis of core/shell GaAs/InGaAs NWs.

The experimental procedure was an insightful view into the work of experimental physicists. In addition to understanding the theoretical construct surrounding NWs, space maps and XRD analysis, it was great to gain some hands on experience in the field of somewhat mere data analysis but also in actual experimentation and active problem solving.

All NW samples measured have been successfully analyzed and revealed useful information about the NW crystal structure. The extracted information (identification of different diffraction signals and out-of-plane strain), together with previous characterizations (SEM, EDX, TEM and ensemble XRD), are essential to the understand the relaxation mechanism and structure of those hetero-systems.

Overall, the experiences I have made during the Summer Program, will without a doubt, embellish my academic and professional development as an individual for the future.

Acknowledgements

I would like to sincerely thank my supervisor Genziana, who so kindly gave me a project of my own to work on in my own time. In addition she was a helpful and attentive supervisor, and was happy to answer any questions I had, even if they were not relevant to my work. Thanks to her, I felt included in the office enviroment, and had a very enjoyable experience.

Many thanks as well to Leila Balaghi and Emmanouil Dimakis (Institute of Ion Beam Physics and Materials Research, Helmholtz-Zentrum Dresden-Rossendorf, in Dresden), Raphael Grifone (P23, PETRA III, DESY), Annika Boehme and Kulkarni Satishkumar (DESY NanoLab), and the P08 team members, who made the nano-XRD measurement possible and prepared and pre-characterized the NW samples.

I would like to thank Olaf Behnke and the rest of the Summer Student Program team, for providing me with this opportunity and organising such a great internship. In particular I would like to thank Olaf for persistently encouraging and recommending extracurricular activites throughout Hamburg, and extended.

Finally, I would like to thank the other summer students for being themselves and

giving me a memory for years to come.

References

[1] $http://photon-science.desy.de/facilities/petra_iii/index_eng.html$, *2017*

[2] D. Spiroska et al.Structural and optical properties of high quality zinc-blende/wurtzite GaAs nanowire heterostrucutres. Phys. Rev.B, 80:245325, 2009

[3] P. Kusch et al. Band gap of wurtzite GaAs: A resonant Raman Study.Phys. Rev. B,86:075317, 2012

[4] https://xrayutilities.sourceforge.io/, accessed 05.09.2017

[5] Als-Nielsen et al. Elements of Modern X-Ray Physics, Ørsted Laboratory, Niels Bohr Institute, Copenhagen University, Demark, 2001

[6] http://www.ioffe.ru/SVA/NSM/Semicond/GaInAs/basic.html, accessed 05.09.2017

[7] $https://en.wikipedia.org/wiki/Bragg\%27s_law$

[8] R.S. Wagner and W.C. Ellis, Vapor-liquid-solid mechanism of single crystal growth. Appl. Phys. Lett., 4:89,1964

[9] C. Colombo, et al. Ga assisted catalyst-free growth mechanism of GaAs nanowires by molecular beam epitaxy. Phys. Rev. B, 77:155326, 2008.